

Electric and magnetic fields effects on the excitonic properties of elliptic core-multishell quantum wires

R. Macêdo¹, J. Costa e Silva¹, Andrey Chaves², G. A. Farias²,
and R. Ferreira³

¹Departamento de Ciências Exatas e Naturais, Universidade Federal Rural do Semi-Árido, Caixa Postal 6030, 59600-900 Mossoró, RN, Brazil

²Departamento de Física, Universidade Federal do Ceará, Caixa Postal 6030, Campus do Pici, 60455-900 Fortaleza, Ceará, Brazil

³Laboratoire Pierre Aigrain, Ecole Normale Supérieure, CNRS UMR 8551, Université P. et M. Curie, Université Paris Diderot, 24 rue Lhomond, F-75005 Paris, France

E-mail: andrey@fisica.ufc.br

Abstract. The effect of eccentricity distortions of core-multishell quantum wires on their electron, hole and exciton states is theoretically investigated. Within the effective mass approximation, the Schrödinger equation is numerically solved for electrons and holes in systems with single and double radial heterostructures, and the exciton binding energy is calculated by means of a variational approach. We show that the energy spectrum of a core-multishell heterostructure with eccentricity distortions, as well as its magnetic field dependence, are very sensitive to the direction of an externally applied electric field, an effect that can be used to identify the eccentricity of the system. For a double heterostructure, the eccentricities of the inner and outer shells play an important role on the excitonic binding energy, specially in the presence of external magnetic fields, and lead to drastic modifications in the oscillator strength.

PACS numbers: 78.67.Lt, 71.35.-y

1. Introduction

The investigation of semiconductor low-dimensional structures has a key role on the development of nanotechnology and future nanoscale devices. Recent advances in growth techniques made possible the fabrication of quantum wire structures, where electrons and holes are confined in two dimensions, with only one free dimension. Quantum wires based on radial semiconductor heterostructures have been successfully used in opto-electronic systems and biological sensors, which require a strong confinement of the charge carriers [1, 2, 3]. Many research groups have used various growth techniques to synthesize quantum wires composed of two different semiconductor materials, forming several types of wire, for example i) core-shell wires, *i.e.* a strand of a semiconductor material covered by a layer of another semiconductor material, ii) core-multishell structures, where a wire is covered by a sequence of layers of other materials, and iii) superlattice nanowires, where a longitudinal superlattice is built by stacking cylindrical blocks of different semiconductor materials [4, 5, 6, 7], just to mention a few. Photoluminescence experiments on GaAs/AlGaAs [8, 9] and InAs/InP [10, 11] core-shell quantum wires have been recently reported, where quantum confinement of the carriers is observed with energies that are in good agreement with theoretical predictions.

In this paper, we present a theoretical study of the excitonic properties of core-multishell (CMS) quantum wires, focusing on the effects of eccentricity distortions of the cylindrical wire structure on the exciton binding energy and on its behavior under external electric and magnetic fields. The main effect of the eccentricity is to create regions of higher curvature and, consequently, lower effective potential, [12, 13] which work as traps to the otherwise circularly symmetric charge carriers wavefunctions. A similar effect is investigated *e.g.* in Ref. [14], though only for electrons, not for excitons, in the so-called prismatic quantum wire, where a hexagonal-like wire exhibits a higher wavefunction distribution over the edges of the hexagon, where the curvature is higher. In this case, the electron energy states exhibit oscillations as the intensity of an axially applied magnetic field increases, which is reminiscent of the Aharonov-Bohm (AB) effect. [14] In fact, the AB effect for electrons in a core-shell wire has been experimentally confirmed by the observation of quantum interference effects on the magnetoresistance of a $\text{In}_2\text{O}_3/\text{InO}_x$ nanowire. [15]

As the exciton has neutral net charge, it is not supposed to be affected by electric/magnetic fields *a priori*. [16] However, electric fields naturally separate electrons and holes wavefunctions, due to their opposite charges, creating regions of non-neutral net charge and affecting the exciton binding energy, [17] through the so-called quantum confined Stark effect (QCSE). Our results show how the carriers energy spectra and exciton binding energy are affected by an applied electric field perpendicular to the wire axis, considering different in-plane directions, which can be used to obtain information about the eccentricity of the wire and its direction of distortion. Such a charge carriers separation does not occur in the case of an axially applied magnetic field, leading to a practically neutral net charge and, consequently, a negligible effect of the field intensity

on the exciton binding energy. On the other hand, the observation of excitonic AB oscillations have been reported in semiconductor quantum *rings* when electrons and holes have an intrinsic spatial separation, due to built-in electric fields or structural effects. [18, 19, 20, 21, 22] In fact, our results demonstrate that in elliptic CMS wires, electrons and holes are pushed to the regions of higher curvature of the confining shell with different strengths, yielding regions of non-neutral charge and, consequently, to an enhancement of the magnetic field effect on the exciton binding energy, which starts to exhibit AB oscillations. The regions of non-neutral charge demonstrated in this paper may also play a role in other geometries of core-shell quantum wires which share the property of exhibiting high curvature regions, such as the semiconductor quantum wires with square, hexagonal and triangular cross sections reported in the literature. [23, 14]

The remainder of the paper is organized as follows: Sec. II presents the theoretical model for calculating the exciton energy. The results for quantum wires containing one or two confining shells are shown and discussed in Sec. III, whereas in Sec. IV we summarize our findings and present our concluding remarks.

2. Theoretical Model

The system we investigate consists of a cylindrical inner wire (core) covered by a sequence of layers of different intercalated materials (shells), as sketched in Fig. 1 (a). In order to help us to study non-circular symmetries of the system, Cartesian coordinates are applied, taking the (x, y) as the confinement plane and z as the free direction. The eccentricity of the elliptic core-multishell structure, which is top viewed in Fig. 1 (b), is defined as $\xi = a/b$. The ellipse is assumed to preserve the same inner area as the original circular shell that generates it. Using the symmetric gauge for the vector potential, $\mathbf{A} = (By/2, -Bx/2, 0)$, the Hamiltonian that describes the system, within the effective mass approximation, reads [24, 25]

$$H_{exc} = \sum_{i=e,h} \left\{ -\frac{\hbar^2}{2m_i^{\parallel}} \left(\vec{\nabla}_{2D,i} - \frac{2\pi}{\Phi_0} \vec{A} \right)^2 + V_i(x_i, y_i) \right\} - \frac{\hbar^2}{2\mu_{\perp}} \frac{\partial^2}{\partial z^2} - \frac{e^2}{\epsilon|\vec{r}_e - \vec{r}_h|}, \quad (1)$$

where the indexes e and h stand for electron and hole, respectively, m_i^{\parallel} is the in plane effective mass of each charge carrier, $\Phi_0 = h/e$ is the magnetic quantum flux, μ_{\perp} is the electron-hole reduced mass in the z -direction, and $z = |z_e - z_h|$ is the electron-hole relative coordinate. The $V_i(x_i, y_i)$ term is the hetero-structure potential, due to the bands mismatches, whereas the last term of Eq. (1) accounts for the electron-hole Coulomb interaction.

The influence of a graded interface between materials has been already investigated by previous papers in the literature, [25] where it was demonstrated that such an interface just leads to slightly larger confinement and excitonic energies, while their dependencies on external magnetic fields or wire dimensions remains essentially

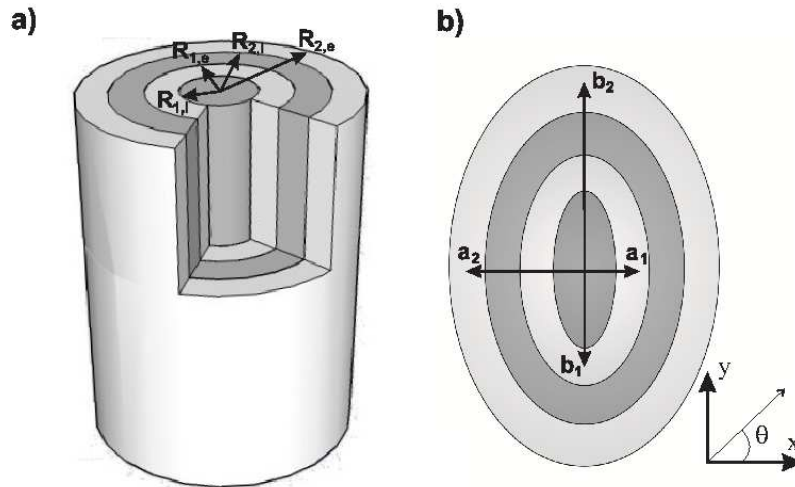


Figure 1. (a) Sketch of a core-multishell structure studied in this work, which is infinitely long in the z -direction and has a radial heterostructure made out of different semiconducting materials, represented by light and dark grey regions. The m -th shell is delimited by inner and outer radii $R_{m,i}$ and $R_{m,e}$. We also investigate elliptic structures, where the eccentricity is defined as $\xi = a_m/b_m$, as illustrated in the top view of the elliptic core-multishell quantum wire in (b).

preserved. In this work, we will consider an abrupt interface between the core and shell layers. Dielectric mismatch effects between materials are also neglected in our model. Previous papers in the literature [26, 27, 28] have demonstrated that these effects are described by potentials that are proportional to $1 - \epsilon_1/\epsilon_2$, where ϵ_1 and ϵ_2 are the dielectric constants of the hetero-structure materials, and are less important for large widths of the hetero-structure layers. The materials involved in the hetero-structures studied in this paper have approximately the same dielectric constant, and the role of the dielectric mismatch effect due to the boundary between the outmost shell and the surrounding medium is ruled out by considering a large width of this shell, therefore, dielectric mismatch effects are negligible to a good approximation in our model. The heterostructure materials considered in this work have also similar lattice constants, so that strain effects does not play an important role as well.

In order to solve the Schrödinger equation for the exciton $H_{exc}\Psi = E_{exc}\Psi$, we neglect initially the coulombic coupling, so that the solutions can be put in the form $\Psi = \psi_e(\vec{\rho}_e)\psi_h(\vec{\rho}_h)\psi_z(z)$ to obtain

$$\left\{ -\frac{1}{m_i^{\parallel}} \left(\vec{\nabla}_{2D,i} - \frac{2\pi}{\Phi_0} \vec{A} \right)^2 + V_i(x_i, y_i) \right\} \psi_i = E_i \psi_i, \quad (2)$$

for each carrier i , whose in-plane position vector is given by $\vec{\rho}_i$. In this equation, and from now onwards, energy variables are divided by the Rydberg energy Ry , spatial variables by the Bohr radius a_0 , and effective masses by the free electron mass m_0 , in order

to make the equations dimensionless. A gauge invariant form of the finite differences scheme is applied to solve for the lowest energy states of this equation numerically, [29] from where one obtains the carriers in-plane wavefunctions ψ_e and ψ_h , which are then integrated along with the Coulomb term to form an effective potential for the problem in the z -direction, yielding

$$\begin{aligned} & -\frac{1}{\mu_{\perp}} \frac{d^2}{dz^2} \psi_z - \frac{2}{\epsilon} \int d\vec{\rho}_e \int d\vec{\rho}_h \frac{|\psi_e|^2 |\psi_h|^2}{\sqrt{(\vec{\rho}_e - \vec{\rho}_h)^2 + z^2}} \psi_z \\ & = E_z \psi_z. \end{aligned} \quad (3)$$

We assume a gaussian wave function [30] as the solution in z

$$\psi_z(z) = \frac{1}{\sqrt{\eta}} \left(\frac{2}{\pi}\right)^{1/4} \exp\left(-\frac{z^2}{\eta^2}\right), \quad (4)$$

where η is the variational parameter that minimizes $E_z = \langle \psi_z | H_z | \psi_z \rangle$, where H_z is the Hamiltonian in the z -direction (see Eq. (3)). Some of the integrals involved in this minimization are analytical, [25] leading to

$$E_z = \frac{1}{\mu_{\perp} \eta^2} - \frac{2}{\epsilon \eta} \sqrt{\frac{2}{\pi}} \int_V |\psi_e|^2 |\psi_h|^2 \exp(a) K_0(a) dV, \quad (5)$$

where $dV = d\vec{\rho}_e d\vec{\rho}_h$, $a = |\vec{\rho}_e - \vec{\rho}_h|^2 / \eta^2$ and $K_0(x)$ is the modified zero-order Bessel function of second kind. The last integral is further calculated numerically, and the exciton energy is obtained by $E_{exc} = E_e + E_h - E_z$. We repeat the variational procedure for different combinations of electron and hole eigenstates and look for the combination of states that lead to the lowest exciton energy E_{exc} , which, as far as the variational method is concerned, represents an upper bound for the exciton ground state energy.

Notice that, rigorously speaking, the best approach to this problem would be not to separate the electron and hole variables, since Eq. (1) is actually non-separable, because of the Coulomb term. However, such an exact approach would lead to a five-dimensional problem (two in-plane coordinates for each electron and hole and a relative z -coordinate for the exciton), which is computationally expensive. Using the electron-hole states basis to construct a matrix that represents the Hamiltonian and then diagonalizing it is not convenient as well, since each matrix element would consist of a five-dimensional integral, and there must be many of them for a properly accurate Hamiltonian. As a matter of fact, these more accurate procedures were used in the literature mostly for circularly symmetric problems, where one can take advantage of the system symmetry to reduce the number of coordinates, or to (semi-)analytically solve for the single-particle eigenstates. [16, 31] Conversely, our case requires Cartesian coordinates, which allows us to investigate elliptic shells, in-plane electric fields, and systems with arbitrary shell geometry, by paying the price of having more coordinates to deal with. Thus, the main idea of the present model is to circumvent this problem by using a much simpler approach, which, in summary, consists in (i) assuming, as an approximation, that one can separate the variables, (ii) solving for the single-particles separately, and then (iii) minimizing the exciton energy as a whole by a variational

procedure. Due to its simplicity, this factorization of the wave function has been widely used in the literature, even in the case of degenerate single particle states, such as in AB oscillations. [32] However, it is worthy to point out that in the degenerate case, this procedure leads to less accurate results, since it does not allow for an excitonic state consisting of an admixture of single-particle eigenstates. Even so, we believe that, despite the model simplicity, the results obtained by the present approximation in the remainder of this paper are accurate enough, and a more sophisticated technique would require great efforts for just small quantitative corrections to the results.

3. Results and Discussions

In the following subsections, we apply our model for the study of the eigenstates and binding energies of systems consisting of a $\text{Al}_{0.3}\text{Ga}_{0.7}\text{As}$ core wire covered by one and two confining GaAs shells, respectively. In our calculations, we assume the dielectric constant of GaAs as $\epsilon = 12.9 \epsilon_0$, the conduction (valence) band offset $V_e = 262 \text{ meV}$ ($V_{hh} = 195 \text{ meV}$), the electron effective mass (assumed to be isotropic) as $m_e^\perp = m_e^\parallel = 0.067 m_0$, and the heavy hole effective mass as $m_{hh}^\perp = 0.11 m_0$ and $m_{hh}^\parallel = 0.51 m_0$. [33, 34]

3.1. Single shell confinement

Let us first consider a $\text{Al}_{0.3}\text{Ga}_{0.7}\text{As}$ core wire, covered by a GaAs/ $\text{Al}_{0.3}\text{Ga}_{0.7}\text{As}$ shell. In this case, the GaAs shell works as a radial quantum well for both electron and hole, which will be preferably confined in this region.

Let us focus initially on the effects of an external electric field applied perpendicularly to the wire axis of a core wire on its energy states. Obviously, in a circular heterostructure, the energy spectrum does not depend on the electric field application direction in the (x, y) -plane. Moreover, as we previously mentioned, the confined states in the circular case are similar to the in-plane states of circular quantum rings, where the influence of an in-plane electric field has already been extensively investigated by previous works in the literature. [35, 17] In the elliptic CMS case, electric fields applied in different directions lead to qualitatively different behaviors of the energy states as a function of the electric field modulus, as illustrated in Fig. 2, for the (a) electron and (b) heavy hole energy states in a $\xi = 0.9$ elliptic CMS, considering an electric field with different application angles θ (we consider $R_{1,i} = 230 \text{ \AA}$ and $R_{1,e} = 330 \text{ \AA}$). More specifically, for a wire squeezed in the x -direction (see Fig. 1), when the electric field is applied in the y -direction ($\theta = \pi/2$), the ground state rapidly decreases with the field (by roughly $eF(R_{1,e} + R_{1,i})/2$), while many crossings are observed between excited states as the field intensity increases, whereas for a field applied in the squeezing direction ($\theta = 0$), the energies just decrease with the field, due to the quantum confined stark effect. [36] Moreover, the energy crossings for electrons and holes happen for different values of electric field, which could help one to identify which carrier is involved in each transition. Actually, the behavior observed in the $\theta = \pi/4$ case is quite similar

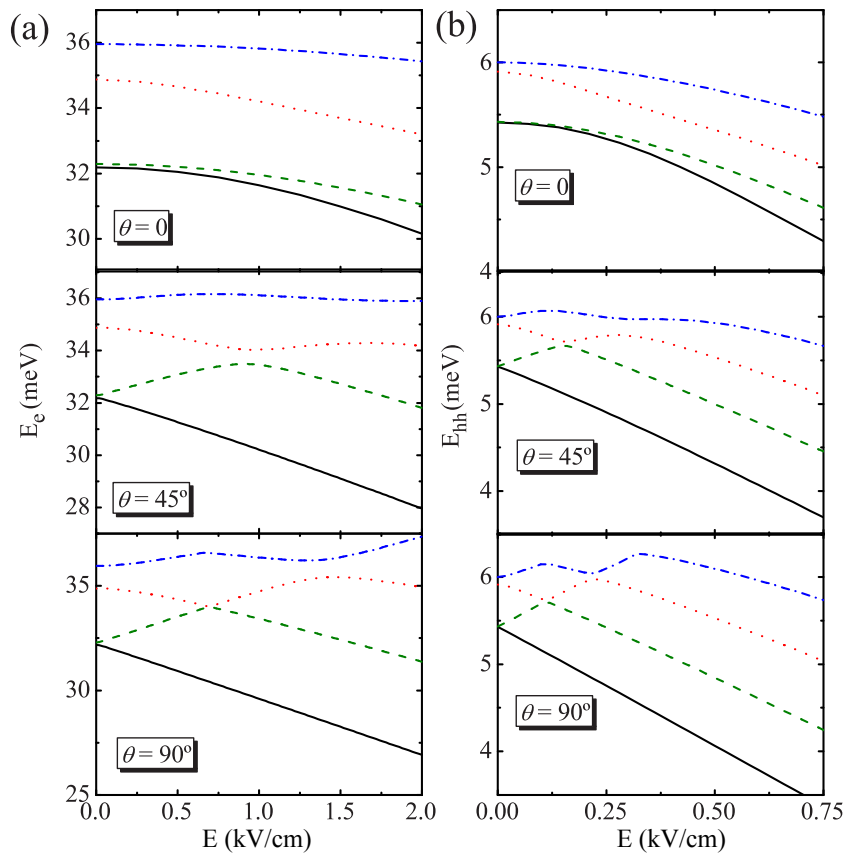


Figure 2. (color online) Confinement energies of (a) electrons and (b) holes in a $\text{Al}_{0.3}\text{Ga}_{0.7}\text{As}/\text{GaAs}/\text{Al}_{0.3}\text{Ga}_{0.7}\text{As}$ radial heterostructure as a function of the in-plane electric field intensity, considering an eccentricity $\xi = 0.9$. The field is applied at three different angles θ from the x -axis.

to the one in stacked double quantum dots under an electric field applied along the dots axis. [37, 38] This is a consequence of the localization of the carriers in the regions of maximum curvature, as illustrated in Fig. 3, so that when the electric field is applied at $\theta = \pi/4$, the system is indeed similar to the double dots case mentioned. So the dependence of the energy levels with both magnitude and orientation of the applied electric field can be used as a tool to infer on the eccentricity of experimentally grown CMS wires, where the presence of crossings between energy states indicates in which direction the higher curvature regions are situated.

By analyzing Fig. 3, it becomes clear that the in-plane wave functions in this system are quite similar to those in quantum rings, as expected. [39, 40, 13] The difference between the two systems concerns the wave functions in z -direction, which are spatially restricted in the latter, but free in the former. As in the rings case, in the presence of an axially applied magnetic field, the eigenenergies of individual carriers display oscillations due to the Aharonov-Bohm effect (not shown, see e.g. Refs. [39, 41]). On the other hand, the exciton is a neutral particle and, as such, should not exhibit response to magnetic fields. Indeed, as one can verify in the Fig. 4 (solid curve), there is

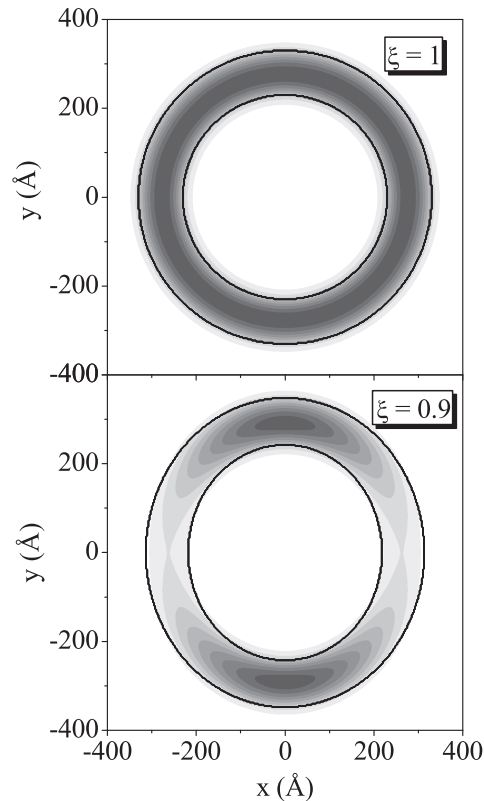


Figure 3. Electron ground state wave functions in (a) circular and (b) $\xi = 0.9$ elliptic $\text{Al}_{0.3}\text{Ga}_{0.7}\text{As}/\text{GaAs}/\text{Al}_{0.3}\text{Ga}_{0.7}\text{As}$ core-multishell quantum wires, considering $R_{1,i} = 230 \text{ \AA}$ and $R_{1,e} = 330 \text{ \AA}$. Similar localization effects are obtained for holes (not shown).

no significant modification of the exciton binding energy as the magnetic field increases for a circular shell. Interestingly enough, the AB effect is significantly enhanced as the eccentricity of the CMS becomes lower than 1. This effect comes from the fact that electron and hole wave functions are not completely overlapped in the elliptic cases shown: the integrated overlap between electron hole for each case were calculated as $\langle \psi_e | \psi_h \rangle \approx 0.999, 0.982$ and 0.984 , for $\xi = 1, 0.95$ and 0.9 , respectively. In the circular case, there is no preferable confinement region along the shell, so that both the electron and hole are distributed equally along the whole GaAs region and the net charge is neutral practically everywhere. The integrated overlap does not reach unity in this case just because their wavefunctions penetration in the barriers are slightly different. However, for a $\xi = 0.95$ elliptic system, the carriers are pushed to the highest curvature regions, and in the proposed CMS, heavy holes are pushed more strongly, due to their heavier mass as compared to that of the electron. Being still not completely confined in the high curvature regions, the electron wavefunction covers a larger region as compared to the hole's wave function, then creating a wide region of suppressed overlap, namely, a non-neutral net charge. As a consequence, the AB effect is enhanced, as shown by the curve with circles in Fig. 4. As the eccentricity value is further decreased to

$\xi = 0.90$, the electron is further compressed towards the high curvature regions and, eventually, electron and hole wavefunctions start to cover similar areas, enhancing again the integrated overlap to $\langle \psi_e | \psi_h \rangle \approx 0.984$. Most importantly, being pushed towards the high curvature regions, the wave functions start losing the ring-like topology of the shell and, consequently, the amplitude of oscillation in the $\xi = 0.95$ case is slightly higher than that of $\xi = 0.9$. Such a reduction in the amplitude of AB oscillations due to the eccentricity of a ring confinement is also observed in the single particle energy spectrum of quantum rings, as reported in Ref. [39].

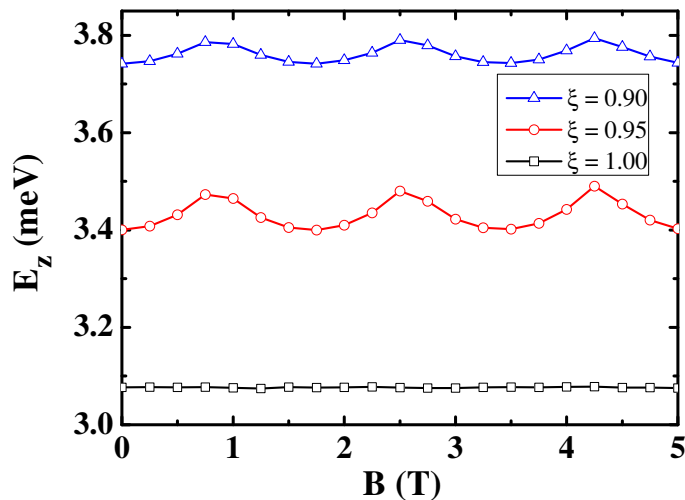


Figure 4. (color online) Exciton binding energies in a $\text{Al}_{0.3}\text{Ga}_{0.7}\text{As}/\text{GaAs}/\text{Al}_{0.3}\text{Ga}_{0.7}\text{As}$ radial heterostructure as a function of the magnetic field for different values of eccentricity: $\xi = 1$ (black squares), 0.95 (red circles) and 0.9 (blue triangles).

The ground state exciton energy as a function of the electric field intensity is shown in Fig. 5 for a $\xi = 0.90$ elliptic quantum ring, considering the same angles of application as in Fig. 2. The zero field binding energy is around 3.74 meV. As the electric field intensity increases, electron and hole are pushed to different directions, leading to a smaller modulus of the exciton binding energy E_z . For a horizontally applied electric field ($\theta = 0$), the exciton binding energy decreases smoothly as the electric field intensity is enhanced. Conversely, for the other application angles, the exciton binding energy decreases abruptly, rapidly converging to ≈ 1.55 meV. Indeed, for $F \parallel x$ carriers should leave the $\theta = \pm\pi/2$ regions and migrate to the $\theta = 0$ (hole) or $\theta = \pi$ (electrons) regions under the action of the field, whereas carriers are already preferably localized along the field in the $F \parallel y$ case.

3.2. Double shell confinement

We now investigate the case of a double shell structure, consisting of an inner $\text{Al}_{0.3}\text{Ga}_{0.7}\text{As}$ wire and two confining (GaAs) shells with the same width $W = 100$ Å,

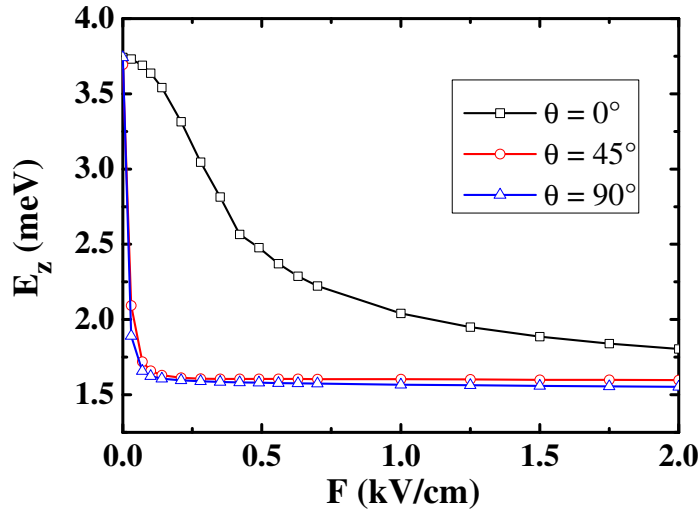


Figure 5. (color online) Exciton binding energies in a $\text{Al}_{0.3}\text{Ga}_{0.7}\text{As}/\text{GaAs}/\text{Al}_{0.3}\text{Ga}_{0.7}\text{As}$ radial elliptic heterostructure, with $\xi = 0.90$ eccentricity, as a function of an in-plane electric field with different application angles θ , where $\theta = 0$ is the horizontal direction in Fig. 1 (b).

separated by a 50 \AA barrier ($\text{Al}_{0.3}\text{Ga}_{0.7}\text{As}$) shell. Let us discuss initially the independent electron and hole states. In the circular case, the radial confinement energies for both shells, separately, are practically the same, exhibiting only a negligible difference due to the angular motion energy term, which is inversely proportional the average radius of each shell. Figure 6 shows the confinement energies and average radii for (a) electrons and (b) heavy holes states in such a structure, as a function of the magnetic field intensity. The hole ground state (solid, black circles) is initially confined in the inner GaAs shell, whereas first (dashed, red squares) and second (dotted, blue triangles) excited states are in the outer one, as one can verify by their average radii in the bottom panel of Fig. 6 (b). This explains the larger period of oscillation of the hole ground state, as compared to the excited ones. As the magnetic field increases, the ground state curve reaches the other curves periodically, and in these degeneracy points, the average radii of these states are switched. For electrons, the situation is slightly different: due to its lighter effective mass, the electron states wave functions spread over both shells for lower magnetic field intensities, so that their average radii end up in the barrier region, as one can see in the bottom panel of Fig. 6 (a). However, for B greater than $\approx 2 \text{ T}$, the ground state stays in the inner shell region, whereas the excited states are pushed to the outer confining shell, explaining their smaller AB period, as compared to the one of the ground state for larger fields, similar to the holes case.

We previously demonstrated that the eccentricity pushes the charge carriers towards the regions of largest curvature of the shell. Hence, when one of the shells is elliptic, it creates an energy imbalance between the inner and outer shells, creating a preferable region of confinement and, consequently, avoiding states that spread over both shells. This effect is expected to smooth out the average radii transitions and the irregularity

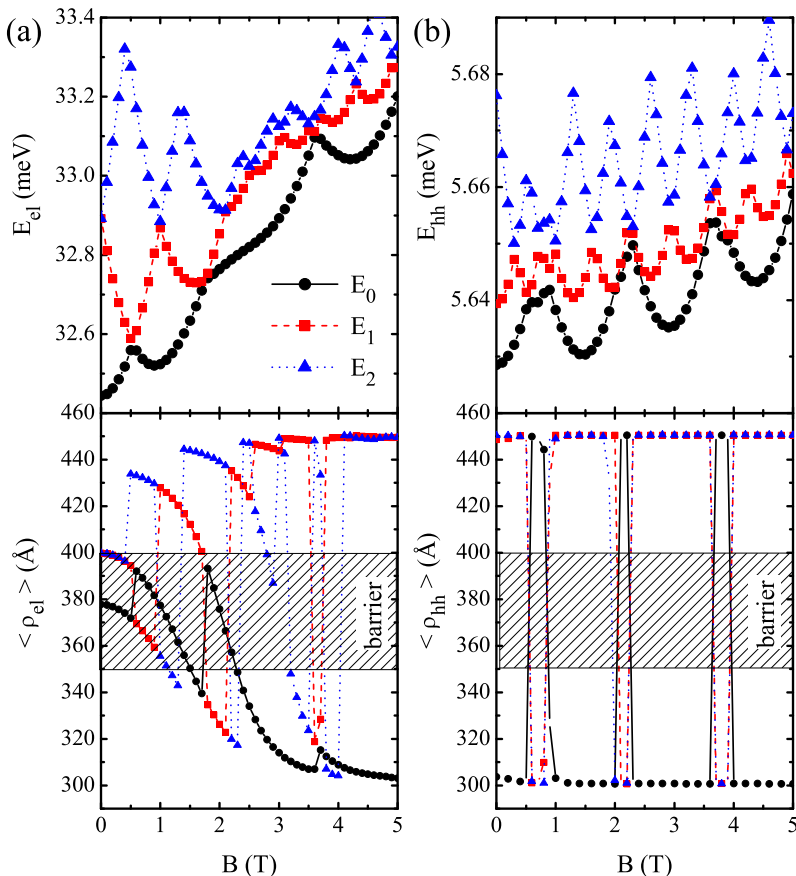


Figure 6. (color online) Confinement energies (top) and average radii (bottom) for the low lying states of (a) electrons and (b) holes in a $\text{Al}_{0.3}\text{Ga}_{0.7}\text{As}/\text{GaAs}$ double shell structure, consisting of a $R_{1,i} = 250 \text{ \AA}$ and $R_{1,e} = 350 \text{ \AA}$ inner shell and a $R_{2,i} = 400 \text{ \AA}$ and $R_{2,e} = 500 \text{ \AA}$ outer shell. The $W = 50 \text{ \AA}$ $\text{Al}_{0.3}\text{Ga}_{0.7}\text{As}$ barrier shell separating the two GaAs confining shells is represented by the shaded area in the bottom panels. Symbols represent the numerical results, and curves are just guides for the eyes.

of the AB oscillations period observed in Fig. 6 for the circular case. This is indeed observed in the results shown in Fig. 7 for the same structure as in Fig. 6, but considering a $\xi = 0.95$ elliptic inner shell. In this case, for any value of magnetic field intensity, ground and first excited states are confined only in the inner shell, whereas second and third (dashed-dotted, green stars) excited states are in the outer one, which can be inferred by the different periods of AB oscillations (top panels), as well as by their average radii (bottom panels).

Actually, the analogous problem of two concentric quantum rings was already investigated in a previous work, [39] though it discusses only the electron states, without mentioning excitonic properties. The carriers eigenstates in the double shell quantum wire are quite similar to those in the double rings case of Ref. [40], which we suggest as a complementary reading for more details about this topic.

The (n,m) overlaps between the wave functions of the n -th electron and the m -th

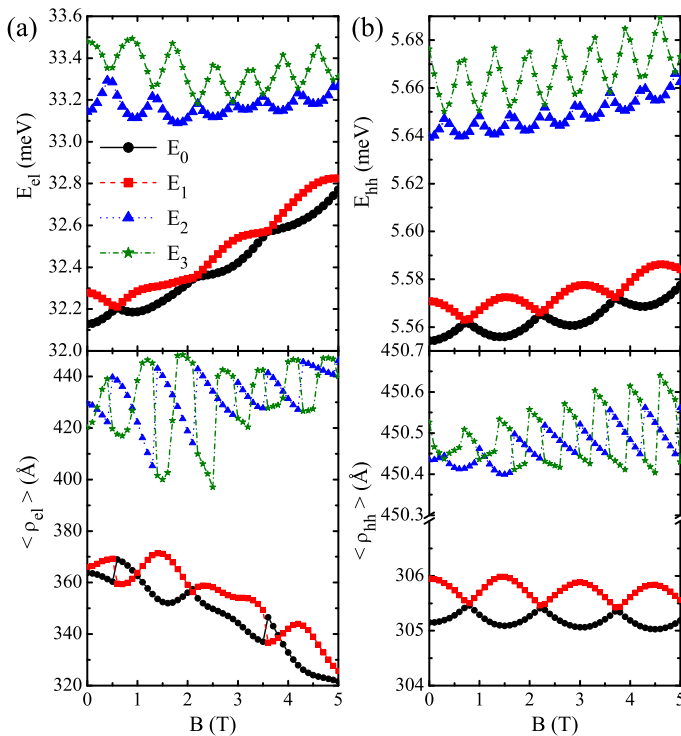


Figure 7. (color online) The same as in Fig. 6, but for a $\xi = 0.95$ elliptic inner shell.

hole eigenstate are shown as a function of the inner shell eccentricity in the Fig. 8, where the ground state exciton binding energy is shown as inset (same CMS as in Figs. 6 and 7, but for $B = F = 0$). As we already mentioned, when both shells are circular, electrons and holes spread over both shells in different ways, due to their different masses and band-offsets. Therefore, in this case, the overlap is small and, consequently, the binding energy of the ground state (0,0) is depreciated. The modulus of the binding energy is enhanced as the inner shell becomes elliptic, followed by the increase of the electron-hole ground state overlap (black squares). Interestingly enough, the (0,1) overlap, between the ground state of the electron and the first excited state of the hole (red triangles), is non-zero only for $\xi > 0.96$, suggesting that electron-hole transitions between these states are allowed only for higher values of eccentricity. Moreover, the (1,0) overlap, between the electron first excited state and the hole ground state (green circles) is zero for any value of ξ , indicating that the electron and hole first excited states are essentially different.

The electron (left panels) and heavy hole (right panels) wave functions shown in Fig. 9, for different values of eccentricity, help us to understand all the features observed in Fig. 8. In the circular case ($\xi = 1$), the ground and first excited states of the hole are of $l_h = 0$ symmetry and related to eigenstates of the radial confinement, localized at the inner and outer shells, respectively. This is analogous to the eigenstates of a double well structure with a large separation barrier, where the ground and first excited states are related to wave functions confined either in one or other of the two wells. On the

other hand, due to its smaller effective mass, the electron tunnels more easily between inner and outer shells, The ground $l_e = 0$ states of the two independent shells hybridize to form roughly radially symmetric and anti-symmetric states. The same holds for the $|l_e| = 1$ states, for which the tunnel coupling is greater, so that, in the end, the ground state of the whole structure ($n = 0$) is the $l_e = 0$ symmetric state while the first excited level ($n = 1$) is the $|l_e| = 1$ symmetric one. Thus, for $\xi = 1$, (i) the (0,0) overlap is non-zero, but it is also lower than 1, because the hole state is entirely confined in the inner shell, whereas the electron state spreads on both shells; (ii) the (0,1) overlap is non-zero, since both states have the same angular symmetry, and differ only by their charge distributions over the inner and outer shells; and (iii) the (1,0) and (1,1) overlaps are zero, since the first excited state of the electron has a different angular symmetry, as compared to both states of the hole. Notice also that the s -like ground state and the p -like first excited electron state for $\xi = 1$ explains why the energy behavior as a function of the magnetic field for this carrier, shown in Fig. 6 (a), looks like an ordinary AB spectrum for $B < 2$ T, where the magnetic field is still not strong enough to induce the electron confinement in the inner shell. This is not the case for holes, where both ground and first excited states are s -like.

Figure 9 (b) and (c) show that for smaller ξ , the elliptic inner shell leads to double dot-like states, as mentioned before in the single shell case, where ground and first excited states concern to symmetric and anti-symmetric wave function distributions over the two regions of higher curvature, for both the electron and the hole. Due to this symmetry issue for $\xi < 0.96$, the ground state of one carrier is orthogonal to the first excited state of the other carrier, leading to zero values of both (1,0) and (0,1) overlaps, which suggests that transitions between these electron and hole states are forbidden only in the elliptic case. Besides, due to the fact that the electron and hole first excited state wave functions exhibit the same symmetry for $\xi < 0.96$, the (1,1) transitions become allowed (non-zero overlap) for this range of ξ .

The average radii transitions observed in the Fig. 6 clearly affects the ground state binding energy in this system, specially because they do not occur in the same way for electrons and holes. Thus, the elliptic distortion of the inner shell would also help to smooth out the irregularity of the binding energy as a function of the magnetic field. Indeed, as one can see in Fig. 10, the electron-hole binding energy E_z responds directly to these average radius jumps, since a different confinement region for each carrier, represented by different average radii in Fig. 6, leads to a lower binding energy modulus. These jumps are suppressed as the inner shell becomes elliptic and, consequently, the abrupt variations in the binding energy are smoothed out.

Notice that in the single shell case discussed previously, electrons and holes were already confined in the same region, so that the exciton naturally had a practically zero net charge and, consequently, exhibited negligible dependence on the magnetic field, which was further enhanced as the shell was made elliptic, due to a slightly different dependence of the carriers confinement on the eccentricity. The opposite happened for the double shell structure: the exciton net charge is naturally non-zero and,

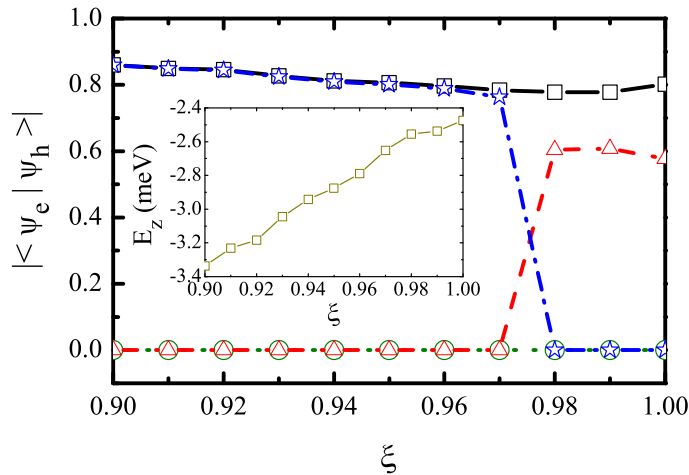


Figure 8. (color online) Overlap between electron and hole wave functions as a function of the inner ring eccentricity, for $B = F = 0$. Overlaps are calculated between the n -th electron state and the m -th hole state, leading to the four (n, m) curves shown, where $(0, 0)$ is represented by squares, $(0, 1)$ by triangles, $(1, 0)$ by circles, and $(1, 1)$ by stars. The straight lines connecting the symbols are guides for the eye. The inset shows ground state exciton binding energies for these eccentricities.

consequently, the binding energy is strongly dependent on the magnetic field, whereas when the inner ring becomes elliptic, it pushes electrons and holes towards the same confinement region, creating an almost zero net charge, which suppresses the influence of the magnetic field on the binding energy.

4. Conclusions

We have investigated the influence of an elliptic distortion of the circular symmetry of core-multishell quantum wires on their confinement energies and excitonic properties. For a single confining shell, increasing the eccentricity leads to a localization of both charge carriers in the points of higher curvature of the system. Under an in-plane electric field applied parallel to the direction of distortion, the energy levels behave as a double dot system, exhibiting energy crossings as a function of the field intensity. When such a field is applied in different directions, these crossings are suppressed. This suggests a way to experimentally probe the eccentricity of a core-multishell wire and its direction of distortion. For a circular CMS quantum wire, the electron and hole are both evenly distributed along the confining shell, creating an effectively neutral exciton which, therefore, does not interact with an axially applied magnetic field. On the other hand, electron and hole wavefunctions are not similarly distributed along the shell in elliptic CMS structures, creating some regions of effectively non-neutral charge. As a consequence, the exciton energy exhibits oscillations as a function of the magnetic field, which is reminiscent of the Aharonov-Bohm (AB) effect, usually observed in quantum rings.

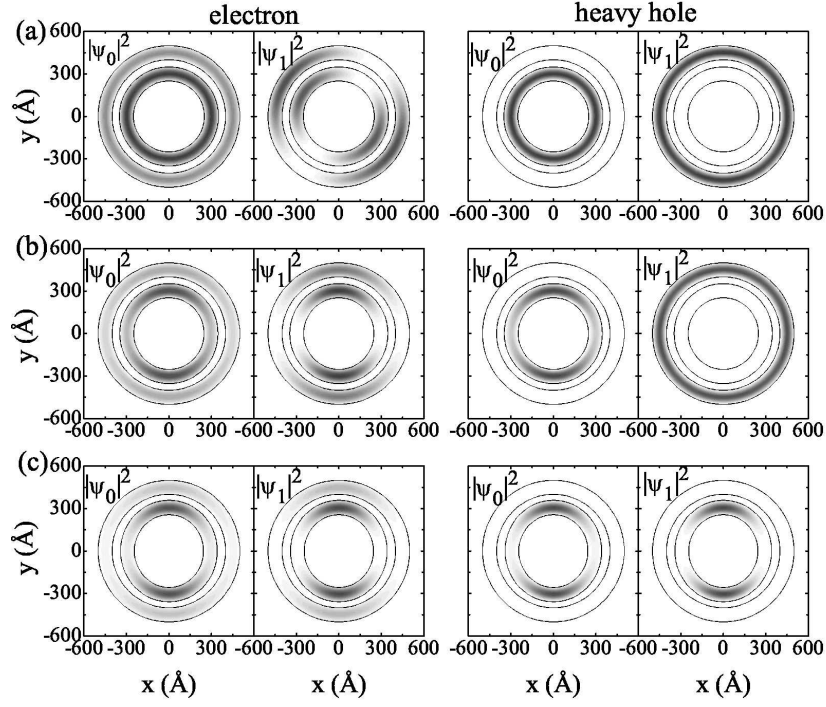


Figure 9. (color online) Electron (left panels) and heavy hole (right panels) wavefunctions for a $R_{1,i} = 250 \text{ \AA}$, $R_{1,e} = 350 \text{ \AA}$, $R_{2,i} = 400 \text{ \AA}$ and $R_{2,e} = 500 \text{ \AA}$ $\text{Al}_{0.3}\text{Ga}_{0.7}\text{As}/\text{GaAs}$ double shell structure, considering different values of the inner ring eccentricity $\xi = 1.0$ (a), 0.98 (b) and 0.95 (c), in the absence of both electric and magnetic fields.

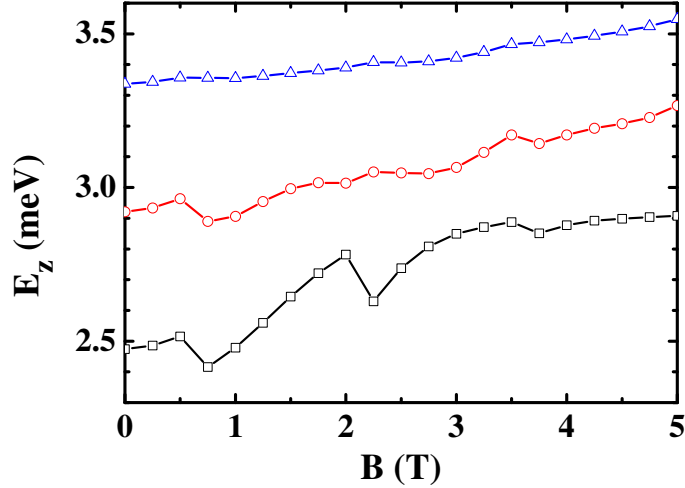


Figure 10. (color online) Exciton binding energies as a function of the magnetic field for a $R_{1,i} = 250 \text{ \AA}$, $R_{1,e} = 350 \text{ \AA}$, $R_{2,i} = 400 \text{ \AA}$ and $R_{2,e} = 500 \text{ \AA}$ $\text{Al}_{0.3}\text{Ga}_{0.7}\text{As}/\text{GaAs}$ double shell structure, considering different values of the inner ring eccentricity ξ .

In the case of two concentric confining shells, we demonstrate that the barrier between the shells plays an important role on the definition of the symmetry of the

electron and hole eigenfunctions. In specific cases, it is possible to observe for one carrier, a ground state wave function that spreads over both shells and a first excited state with non-zero angular momentum, whereas for the other carrier, each eigenstate is confined in a single shell and both have zero angular momentum. This has a drastic effect not only on the behavior of the energy spectrum of each carrier under an external magnetic field, but also on the transition probabilities between electron and hole states. However, considering an elliptic inner shell, even for eccentricities as small as $\xi = 0.95$, the electron and hole states become more similar, as both are confined in the higher curvature regions. In this case, AB oscillations of the carriers energies are more clear, and overlaps between their ground states wave functions are enhanced. Besides, due to the strong confinement of electrons and holes in these higher curvature regions, the exciton binding energy becomes less susceptible to external magnetic fields. Therefore, the inter-shell barrier is demonstrated to be a useful parameter to tune the allowance of transitions between electrons and hole states in the circular case, whereas the eccentricity of the inner ring can be used to push electron and hole wave functions to the same confinement regions, smoothening out the dependence of the exciton binding energy on the external magnetic field.

Acknowledgments

This work has received financial support from the Brazilian National Research Council (CNPq), Fundação Cearense de Apoio ao Desenvolvimento Científico e Tecnológico (Funcap).

References

- [1] Appell D 2002 *Nature* **419** 553
- [2] Cui Y, Wei Q, Park H and Lieber C M 2001 *Science* **293** 1289
- [3] Law M, Goldberger J and Yang P 2004 *Annu. Rev. Mater. Res.* **34** 83
- [4] Choi H J, Johnson J C, He R, Lee S K, Kim F, Pauzuskie P, Goldberger J, Saykally R J and Yang P 2003 *J. Phys. Chem. B* **107** 8721
- [5] Goldberger J, He R, Zhang Y, Lee S, Yan H, Choi H J and Yang P 2003 *Nature* **422** 599
- [6] Wu Y, Fan R and Yang P 2002 *Nano Lett.* **2** 83
- [7] Lauthon L J, Gudiksen M S, Wang D and Lieber C M 2002 *Nature* **420** 57
- [8] Kang J H, Gao Q, Joyce H J, Tan H H, Jagadish C, Kim Y, Guo Y, Xu H, Zou J, Fickenscher M A, Smith L M, Jackson H E and Yarrison-Rice J M 2011 *Cryst. Growth Des.* **11** 3109
- [9] Fickenscher M A, Jackson H E, Smith L M, Yarrison-Rice J M, Kang J H, Paiman S, Gao Q, Tan H H and Jagadish C 2011 *Appl. Phys. Lett.* **99** 263110
- [10] Zanolli Z, Pistol M E, Fröberg L E and Samuelson L 2007 *J. Phys.: Condens. Matter* **19** 295219
- [11] Mohan P, Motohisa J and Fukui T 2006 *Appl. Phys. Lett.* **88** 133105
- [12] da Costa R C T 1981 *Phys. Rev. A* **23** 1982
- [13] Gridin D, Adamou A T I and Craster R V 2004 *Phys. Rev. B* **69** 155317
- [14] Ferrari G, Goldoni G, Bertoni A, Cuoghi G and Molinari E 2009 *Nano Lett.* **9** 1631
- [15] Jung M, Lee J S, Song W, Kim Y H, Lee S D, Kim N, Park J, Choi M S, Katsumoto S, Lee H and Kim J 2008 *Nanoletters* **8** 3189
- [16] Song J and Ulloa S E 2001 *Physical Review B* **63** 125302

- [17] Maslov A V and Citrin D S 2003 *Phys. Rev. B* **67** 121304(R)
- [18] Hu H, Zhu J L, Li D J and Xiong J J 2001 *Phys. Rev. B* **63** 195307
- [19] González-Santander C, Domínguez-Adame F and Römer R A 2011 *Phys. Rev. B* **84** 235103
- [20] Teodoro M D, Campo Jr V L, Lopez-Richard V, Marega Jr E, Marques G E, Gobato Y G, Iikawa F, Brasil M J S P, AbuWaar Z Y, Dorogan V G, Mazur Yu I, Benamara M and Salamo G J 2010 *Phys. Rev. Lett.* **104** 086401
- [21] Li B and Peeters F M 2011 *Phys. Rev. B* **83** 115448
- [22] Miyamoto S, Moutanabbir O, Ishikawa T, Eto M, Haller E E, Sawano K, Shiraki Y and Itoh K M 2010 *Phys. Rev. B* **82** 073306
- [23] Fortuna S A and Li X 2010 *Semicond. Sci. Technol.* **25** 024005
- [24] Peeters F M and Schweigert V A 1996 *Phys. Rev. B* **53** 1468
- [25] Costa e Silva J, Chaves A, Freire J A K, Freire V N and Farias G A 2006 *Phys. Rev. B* **74** 085317; Costa e Silva J, Chaves A, Freire J A K, Freire V N, Degani M H and Farias G A 2007 *J. Mat. Sci.* **42** 2314
- [26] Li B, Slachmuylders A F, Partoens B, Magnus W and Peeters F M 2008 *Phys. Rev. B* **77** 115335
- [27] Slachmuylders A F, Partoens B, Magnus W and Peeters F M 2006 *Phys. Rev. B* **74** 235321
- [28] Sousa A A, Pereira T A S, Chaves A, de Sousa J S and Farias G A 2012 *Appl. Phys. Lett.* **100** 211601
- [29] Governale M and Ungarelli C 1998 *Phys. Rev. B* **58** 7816
- [30] Madarasz F L, Szmulowicz F, Hopkins F K and Dorsey D L 1994 *Phys. Rev. B* **49** 13528
- [31] Mehran Bagheri 2010 *J. Phys. D: Appl. Phys.* **43** 272003
- [32] Janssens K L, Partoens, B and Peeters, F M 2002 *Phys. Rev. B* **66** 075314
- [33] Pavesi L and Guzzi M 1994 *J. Appl. Phys.* **75** 4779
- [34] Yamagiwa M, Sumita N, Minami F and Koguchi N 2004 *J. Lumin.* **108** 379
- [35] Culchac F J, Porrás-Montenegro N and Latgé A 2008 *J. Phys.: Condens. Matter* **20** 285215
- [36] Chaves A, Costa e Silva J, Freire J A K and Farias G A 2007 *J. Appl. Phys.* **101** 113703
- [37] Ferreira R and Bastard G 1997 *Rep. Prog. Phys.* **60** 345
- [38] Sheng W and Leburton J P 2001 *Appl. Phys. Lett.* **78** 1258
- [39] Farias G A, Degani M H, Freire J A K, Costa e Silva J and Ferreira R 2008 *Phys. Rev. B* **77** 085316
- [40] Costa e Silva J, Chaves A, Degani M H, Farias G A and Ferreira R 2011 *Solid State Comm.* **151** 1200
- [41] Wendler L, Fomin V M and Krokhin A A 1994 *Phys. Rev. B* **50** 4642